Chapter 3

Wheel-Rail Impact by a Wheel Flat

Lin Jing

Additional information is available at the end of the chapter

http://dx.doi.org/10.5772/intechopen.70460

Abstract

The finite element method (FEM)-based wheel-rail rolling contact model with a fresh wheel flat was built to investigate the wheel-rail impact responses, where a comprehensive dynamic explicit algorithm was employed. Two basic dynamic effects (i.e., inertia effect and strain-rate effect) and temperature effect during the wheel-rail sliding process were considered. Influences of train speed, flat length and axle load on the wheel-rail impact responses were discussed in terms of wheel-rail impact force, von Mises equivalent stress, equivalent plastic strain and XY shear stress. Simulation results demonstrate that the FEM-based wheel-rail rolling contact model can well describe the strong nonlinearities in geometry, contact and material. The strain rate effect contributes to elevate the maximum von Mises equivalent stress and restrain the plastic deformation. The initial thermal stress can decrease the maximum von Mises equivalent stresses and maximum XY shear stresses, but can aggravate the plastic deformation. Furthermore, the flat-induced wheel-rail impact force, von Mises equivalent stress, equivalent plastic strain and XY shear stress are revealed to be sensitive to train speed, flat length and axle load.

Keywords: wheel flat, impact response, strain rate, finite element simulation, high-speed railway

1. Introduction

The wheel-rail interaction has become increasingly one of the most attractive and important topics in the field of rail transportation, since the serious wheel/rail failure will surely lead to a series of disasters [1, 2]. The wheel flat is a main type of potential dangerous factors of

inducing the wheel/rail failure, which is usually generated by the two following factors: (i) the sudden lock of a running wheel during the braking process, resulting that the braking force exceeds temporarily the available wheel-rail friction force; and (ii) the sliding of the wheel on the rail under the circumstance of a local reduction of the wheel-rail adhesion force [3–5]. **Figure 1** shows a typical photograph of a wheel flat formed by wheel-rail sliding.

The consequences of flat-caused contact irregularity are to excite the significantly larger wheel-rail impact forces than the corresponding quasi-static wheel-loads. The resulted high impact forces may cause severe damages to both railway vehicles and track, including broken axles and axle boxes, damaged bearings, cracks penetrating into the wheels and rail fracture with the risk of derailment [6]. Besides, the presence of wheel flats will produce excessive noises and higher-frequency forced vibrations.

The wheel flat problem remains of great current research interest. This is because that the speeding-up and high-speed trains are expected to be gradually operated on the limit of the possible wheel-rail tractions in accelerating and decelerating, based on optimized and tight time schedules [5, 6]. Furthermore, there are two criteria for determining the allowable value of flat length at present [6]: one is the force-based criterion, which is based on the principle of impact load detectors in the track, and the other is the geometry-based criterion, which specifies an allowable length or depth (or a combination of both), of the flat spot. However, the force-based criterion does not match with the geometry-based criterion, attributed to the fact that there is no unique corresponding relationship between the flat length and the maximum wheel-rail impact force, especially for the high-speed case [5, 7]. Therefore, the wheel-rail impact problem due to the wheel flat needs to be further in-depth studied, so as to provide valuable management decisions, based on better understanding of corresponding regularities and mechanisms.

Figure 1. Photograph of a wheel flat formed by wheel-rail sliding [6].

http://dx.doi.org/10.5772/intechopen.70460

2. Overview of wheel-rail impact problem

The wheel-rail impact problem induced by a wheel flat is usually simulated using the multi-body dynamics (MBD) approach [8, 9] and newly-developed finite element method (FEM) [10, 11]. Then the wheel flat is directly geometrically modeling or simulated by implementing a relative displacement excitation between the wheel and rail [8]. Considering a wheel with a flat rolling on the rail shown in **Figure 2 (a)** and **(b)**, the relative displacement excitations for the wheel flat can be represented by the vertical movement of the wheel center x_0 (positive downwards), which is given approximately by

$$x_0 = \begin{cases} z_0^2/2r & 0 \le z_0 \le l/2 \\ (l - z_0)^2/2r & l/2 < z_0 \le l \end{cases} \tag{1}$$

and

$$x_0 = \begin{cases} 4d\ (z_0/l)^2 & 0 \le z_0 \le l/2 \\ 4d\ ((l - z_0)/l)^2 & l/2 < z_0 \le l \end{cases} \tag{2}$$

for the fresh and rounded flats, respectively; where, $z_0 = r\theta$ is the longitudinal position of the wheel center, and r is the radius of the wheel; l and d is the length and depth of the flat, respectively.

The MBD approaches are well-qualified for the low-frequency dynamics analyses, but they are not suitable for the high-frequency (beyond 20 Hz) dynamics analyses due to the assumptions of rigid bodies [11]. Although the dynamic contact forces were also calculated by the MBD approach with implemented the rolling contact models [12, 13], most of the rolling

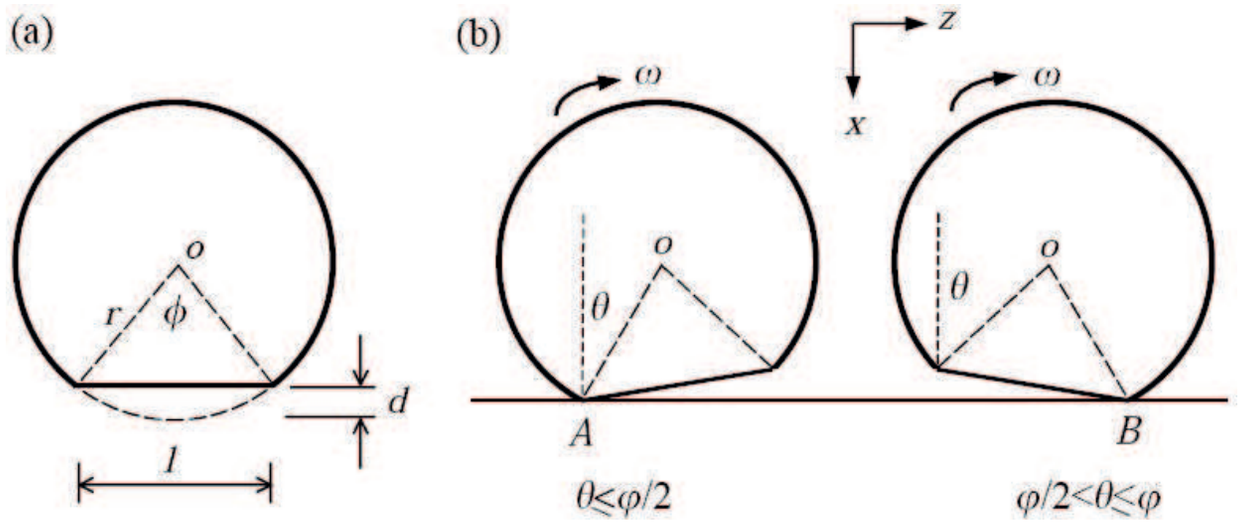

Figure 2. Schematic diagram of the rolling of a wheel with a flat on the rail [8].

contact theories were based on the Hertzian contact and steady rolling assumptions. These assumptions are difficult to describe accurately the wheel-rail impact behavior due to its nonlinearities of materials and the dynamic contact. Besides, the MBD approaches are failed to solve directly the wheel-rail contact stress and strain states, and the dynamic effects are usually ignored to a large extent. Nevertheless, the FEM-based wheel-rail rolling contact simulations have abilities of representing the actual geometrical and kinematic characteristics of the wheel-rail system, and considering the strong nonlinearities in geometry, contact and material [5, 7]. The FEM is therefore more widely-used in wheel-rail impact simulations. It should be noted that, under the high-speed condition, the inertia effect cannot be neglected and the strain rate effect of materials becomes more and more important then. Besides, the thermal stress induced by induced by the friction temperature rising during the wheel-rail sliding process will play a more important role in the wheel-rail interaction.

3. FEM-based wheel-rail rolling contact model

The entire finite element model of the wheel-rail system, built by using commercial software Hypermesh, consists of two wheels (the one has a fresh flat), one axle and two rails. The wheel with the radius of 430 mm has a S1002CN tread, while the rail with a base slope of 1: 40 is the 60 kg/m rail. The whole structure except the substructure below the rail of the wheel-rail system was modeled, and a typical 3-D wheel-rail rolling contact model with a flat length of 40 mm was presented in **Figure 3**, where the width of the flat is equal to 25 mm. To balance the computational precision and efficiency, the contact area of the wheel flat was fined meshed with the size of 4 mm × 4 mm, while the other areas were medially meshed. The entire model was mesh into the 8-node solid element, and comprises 516,629 nodes and 479,038 elements.

The mechanical behaviors of all the wheel-rail components were described by a plastic kinematic hardening constitutive model *MAT_PLASTIC_KINEMATIC [5, 7], where mechanical parameters used in the rolling contact simulations were listed in **Table 1**. Nodal all-DOFs (degree of freedom) constraints were imposed to the bottom of rails, to represent the clamped

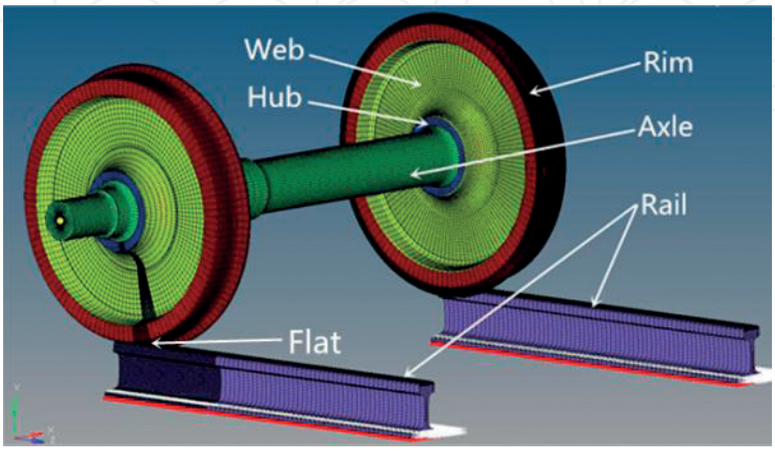

Figure 3. FE model of the wheel-rail system with a 40 mm flat.

Component	Elastic modulus (GPa)	Density (kg/m^3)	Poisson ratio	Yield stress (MPa)	Tangent modulus (GPa)
Rim	213	7800	0.3	561	21
Web	216	7800	0.3	395	21
Hub	213	7800	0.3	417	21
Axle	206	7800	0.3	560	21
Rail	193	7800	0.3	525	19

Table 1. Material parameters used in the rolling contact simulations.

boundary condition, and an axial translational constraint was set to all nodes of the axle. The gravitational acceleration was considered and endowed to all the wheel-rail components. Based on the criterion of EN13104 [14], the static wheel-loads were equivalent to two concentrated forces applied to the two ends of the axle. The initial velocity of the wheel set was endowed by an equivalent translational velocity for both wheels and the axle, and a corresponding rotational velocity only for wheels. An automatic surface-to-surface contact option with the penalty method was generally used for the whole wheel-rail system, to solve the wheel-rail rolling contact.

4. Wheel-rail impact simulation: inertia effect

The whole dynamic wheel-rail impact response process was simulated using finite element code LS-DYNA 3D explicit algorithm, where the inertia effect is considered automatically by the following dynamic equilibrium equation [15].

$$[M]\{\ddot{u}\} + [C]\{\dot{u}\} + [K]\{u\} = \{F\} \tag{3}$$

where [**M**], [**C**] and [**K**] are the structural mass, damping and stiffness matrixes, respectively; $\{u\}$ and $\{F\}$ are the nodal displacement and applied load vectors, respectively.

The maximum vertical wheel-rail impact forces induced by a wheel flat are plotted in **Figure 4** as a function of train speed and flat length. For a given flat length, the non-monotonic relationships between the maximum vertical impact force and train speed are clearly presented, and the peak values of maximum vertical impact forces occur at train speed of 150 km/h. This non-monotonic relationship between the peak vertical force and train speed may be related with the loss of contact under different speeds. For a given train speed, the maximum vertical impact force non-linearly increases with the flat length, and the influence of flat length on the maximum vertical impact force seems to be significant within the speed range from 150 to 250 km/h. For a given flat length and train speed, the influence of axle load on the wheel-rail impact response can be also examined. The maximum vertical impact forces are increased with the axle load for each flat length case.

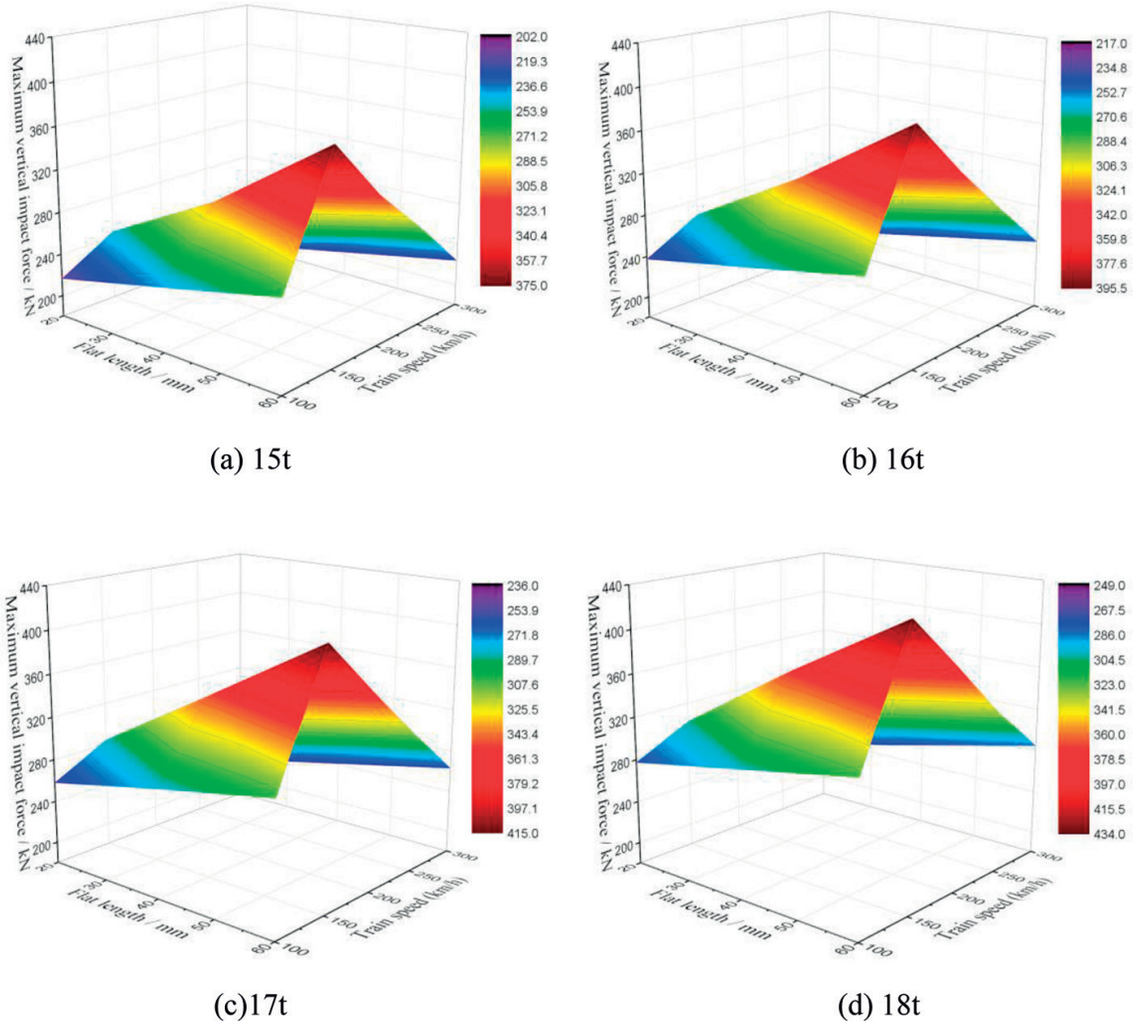

Figure 4. Maximum flat-induced wheel-rail impact forces as a function of train speed and flat length. (a) 15t, (b) 16t, (c) 17t and (d) 18t.

5. Wheel-rail impact simulation: inertia effect + strain rate effect

As stated earlier, the strain rate effect of wheel/rail materials should be taken into account in wheel-rail impact simulations with the continuous raising of train speed. Thus, the strain rate effect is considered in material models of LS-DYNA via inputting the corresponding strain rate-dependent parameters, which are obtained from the quasi-static compressive and split Hopkinson pressure bar tests at a wide range of strain rates. In the present case, the Cowper-Symonds model which scales the yield stress by a following strain rate dependent factor is employed.

$$1 + \left(\frac{\dot{\varepsilon}}{C}\right)^{1/P} \tag{4}$$

where $\dot{\varepsilon}$ is the strain rate, C and P are two strain rate parameters, corresponds to the strain rate parameter,C, (SRC) and strain rate parameter,P, (SRP) options in the material model,

respectively. Based on the experimental fitting [16, 17], the strain rate sensitive material parameters in the present study are set as: C = 45,635 s^{-1} and P = 3.21 for the rim steel and C = 1733 s^{-1} and P = 0.30 for the rail steel, respectively.

The typical vertical wheel-rail impact force history curves, obtained from simulations with or without strain rate-dependent parameters, for the condition of train speed of 200 km/h, flat length of 40 mm and axle load of 17t, are plotted in **Figure 5**. It is clear that the vertical wheel-rail impact force responses derived from both strain rate-dependent and rate-independent

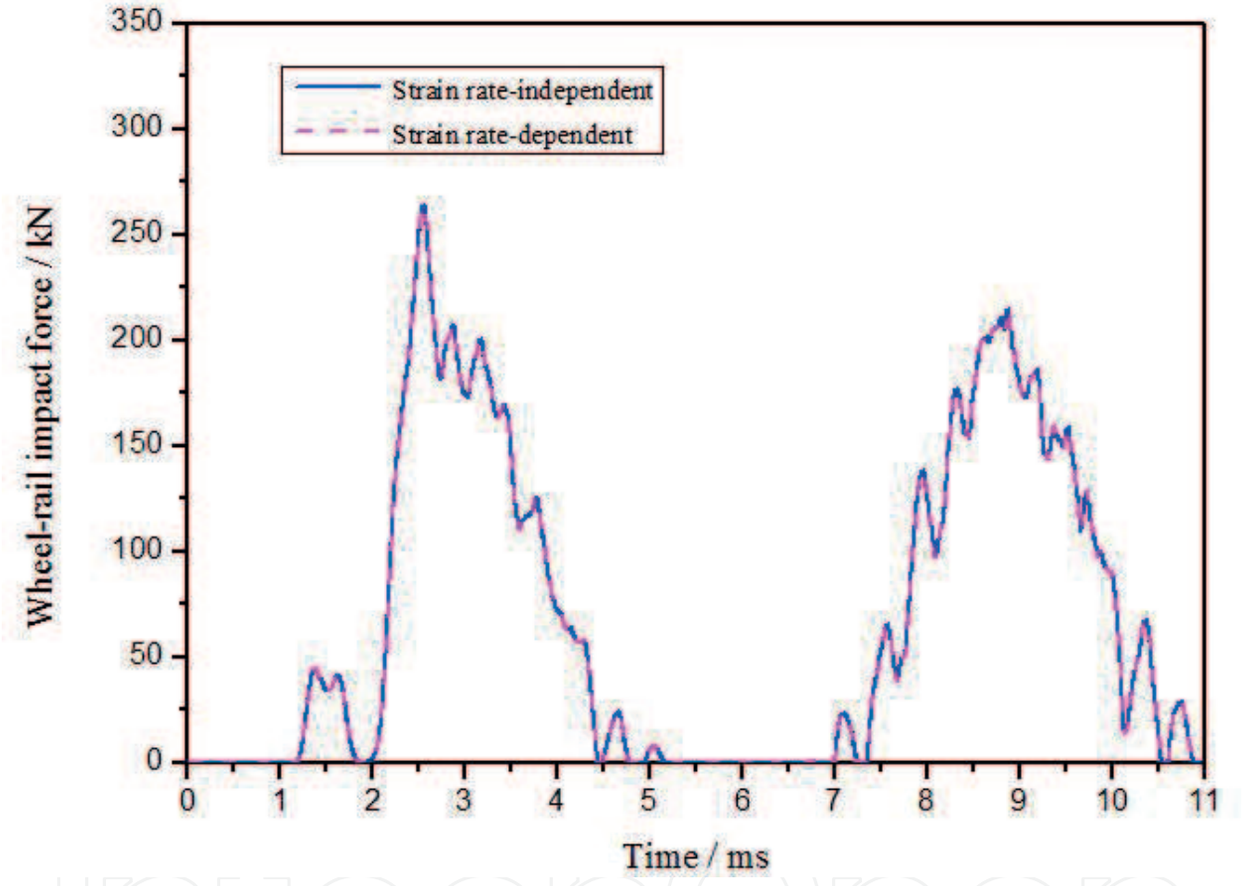

Figure 5. Wheel-rail impact force history curves (17t axle load, 200 km/h train speed and 40 mm flat).

simulations are coincident. This is to say, the strain rate effect of wheel/rail materials has no influence on the vertical impact force response. The first peak impact force with the amplitude of 265 kN, which is generated by the impact of wheel flat against the rail, occurs at 2.6 ms. This impact load is carried directly by the rail, especially for the wheel-rail contact area, since the impact force had no time to transfer to the infrastructure below the rail during the very short time. As a result, the large impact load may induce the plastic deformation and fatigue failure of the wheel and rail.

The typical von Mises equivalent stress, XY shear stress and equivalent plastic strain responses during the wheel-rail impact process derived from both rate-dependent and rate-independent simulations are plotted in **Figures 6–8**, respectively. It is seen from **Figures 6** and **7** that

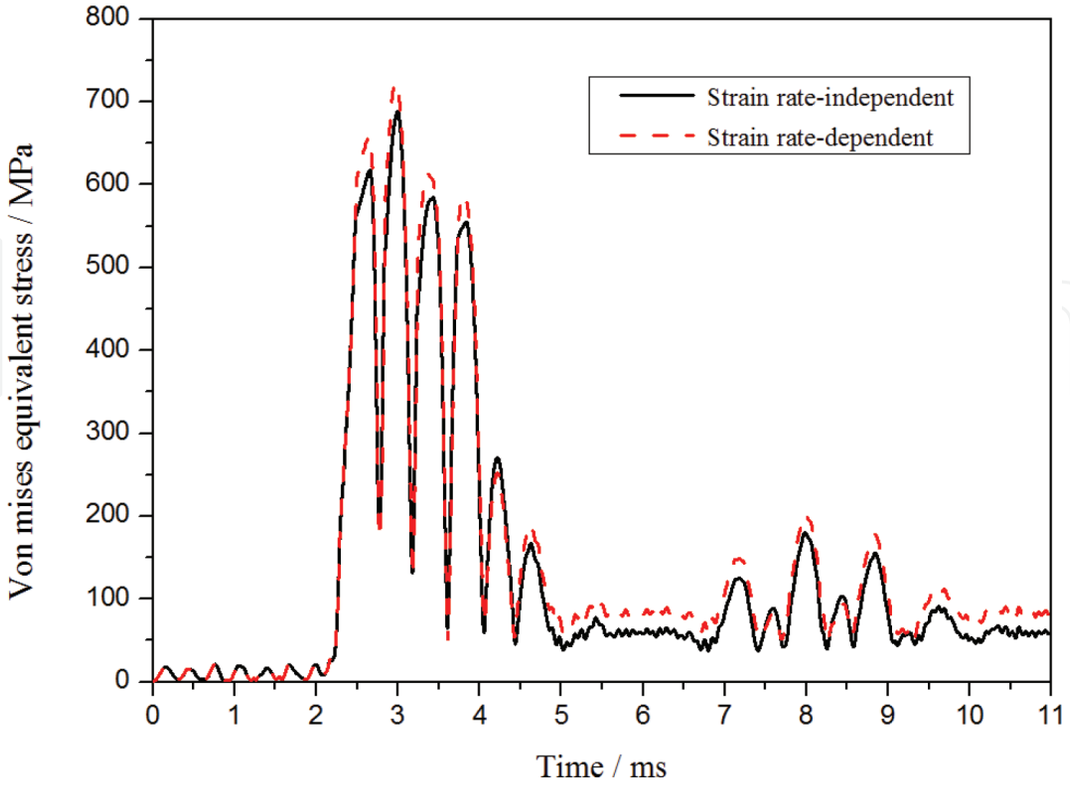

Figure 6. Von Mises equivalent stress history curves (17t axle load, 200 km/h train speed and 40 mm flat).

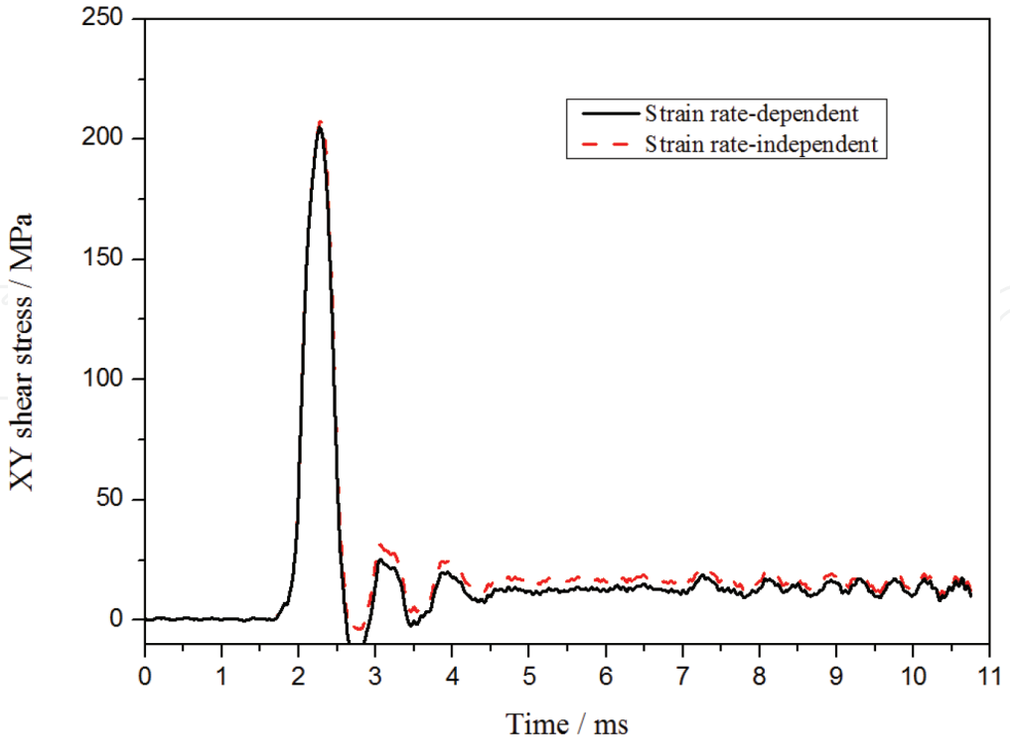

Figure 7. XY shear stress versus time curves (17t axle load, 200 km/h train speed and 40 mm flat).

http://dx.doi.org/10.5772/intechopen.70460

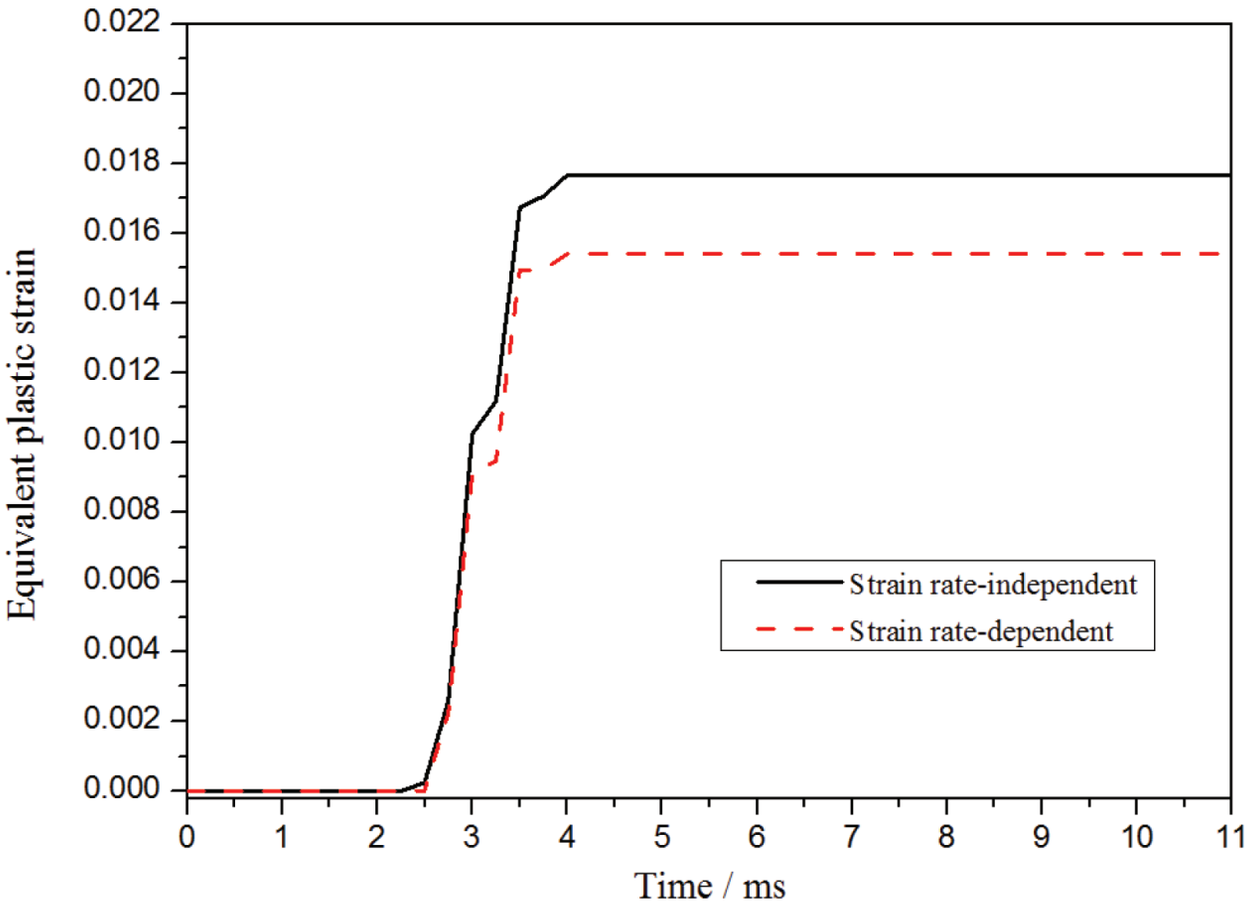

Figure 8. Equivalent plastic strain history curves (17t axle load, 200 km/h train speed and 40 mm flat).

both the von Mises equivalent stress and XY shear stress are significantly larger when the strain rate effect of wheel/rail materials is considered, while from **Figure 8** that the equivalent plastic strain gives an obviously lower value for the strain rate-dependent simulations. These indicate that the von Mises equivalent stress, shear stress and equivalent plastic strain are sensitive to the strain rate, and the hardening effect of the strain rate results the higher von Mises equivalent stress and shear stress, but the lower equivalent plastic strain.

6. Wheel-rail impact simulation: dynamic effects + temperature effect

In this section, the friction temperature rising during the wheel-rail sliding process is also considered in the wheel-rail impact simulation, together with inertia effect and strain rate effect. Thermal stress fields of the wheel and rail, derived from the thermal analysis [5], are inputted to the wheel-rail rolling contact finite element model as an initial pre-stress.

6.1. Typical characteristics of wheel-rail impact responses

Figures 9–11 present a typical set of wheel-rail impact force, von Mises equivalent stress and equivalent plastic strain history curves for the condition of train speed of 200 km/h, flat length

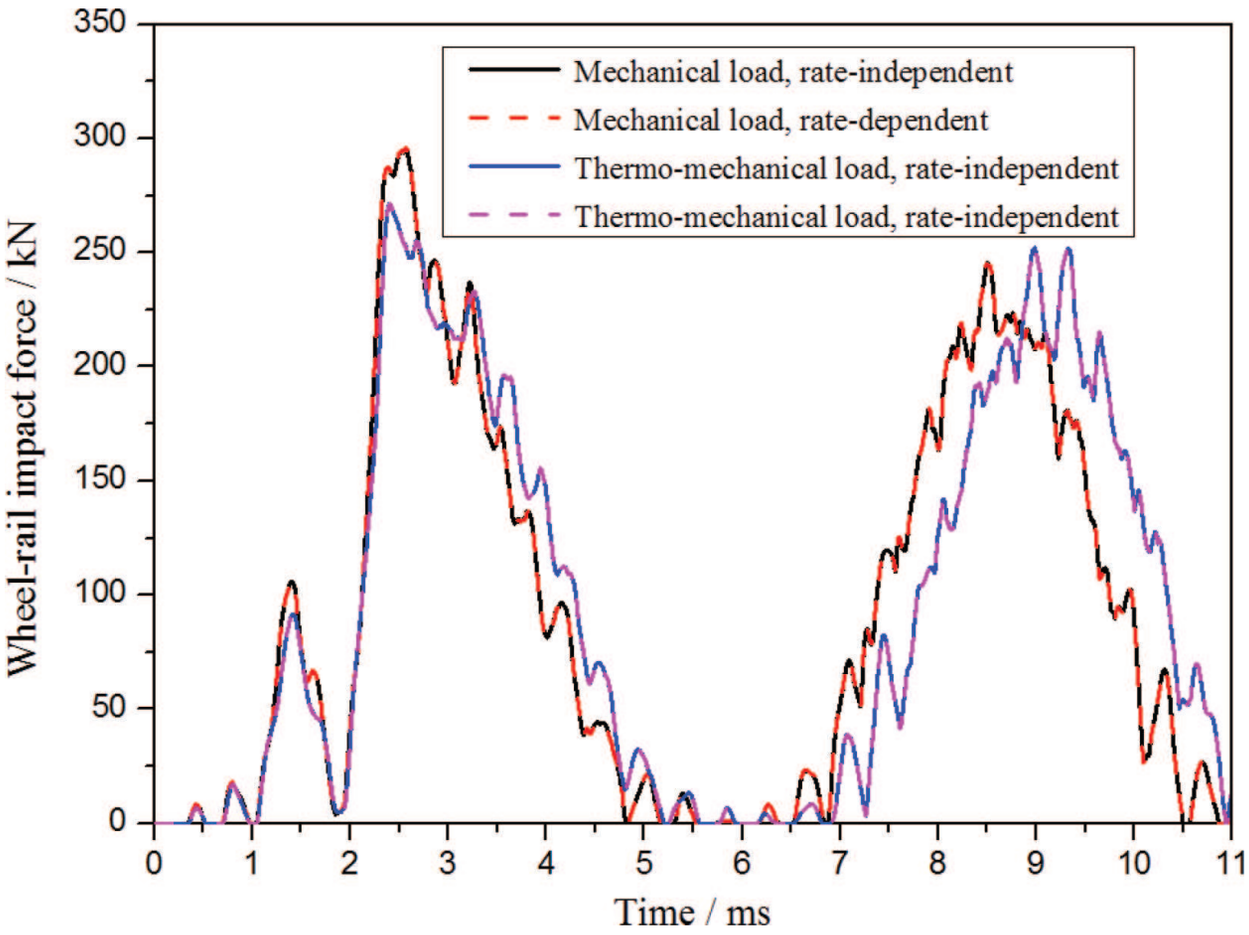

Figure 9. Wheel-rail impact force history curves under mechanical and thermo-mechanical loads.

of 40 mm and axle load of 17t, under mechanical and thermo-mechanical loads, respectively. It is seen from **Figure 9** that the starting times (at ~1.9 ms) and the moments corresponding to the peak forces (at ~2.5 ms) of the wheel-rail impact induced by a flat under four conditions are almost the same, in other words, both quantities are regardless of the thermal load (stress) and strain rate. However, after the occurrence of the wheel-rail impact, the initial thermal stress contributes to prolong the duration of wheel-rail impact and the duration of the second dropping of the wheel, due to the weakening of the stiffness of both wheel and rail caused by the initial thermal stresses. Besides, the wheel-rail impact force responses under either mechanical or thermo-mechanical loads are independent with the strain rate. However, the peak values of the wheel-rail impact force under thermo-mechanical load are slightly lower than those under pure mechanical load. This is the consequent of the increasing impact duration under thermo-mechanical load for a given initial momentum of the wheel.

From **Figure 10**, the change tendencies of the von Mises equivalent stress history curves under four conditions are similar, but the peak values present certain sensitivity to the initial thermal load (stress) and strain rate. The peak von Mises equivalent stress under pure mechanical load with the strain rate considered is the largest, and then that under pure mechanical load without considering strain rate, following by that under thermo-mechanical load with considering the strain rate, and that under thermo-mechanical load without considering strain rate is the smallest. Obviously, the superposition of the initial thermal stress and mechanical stress

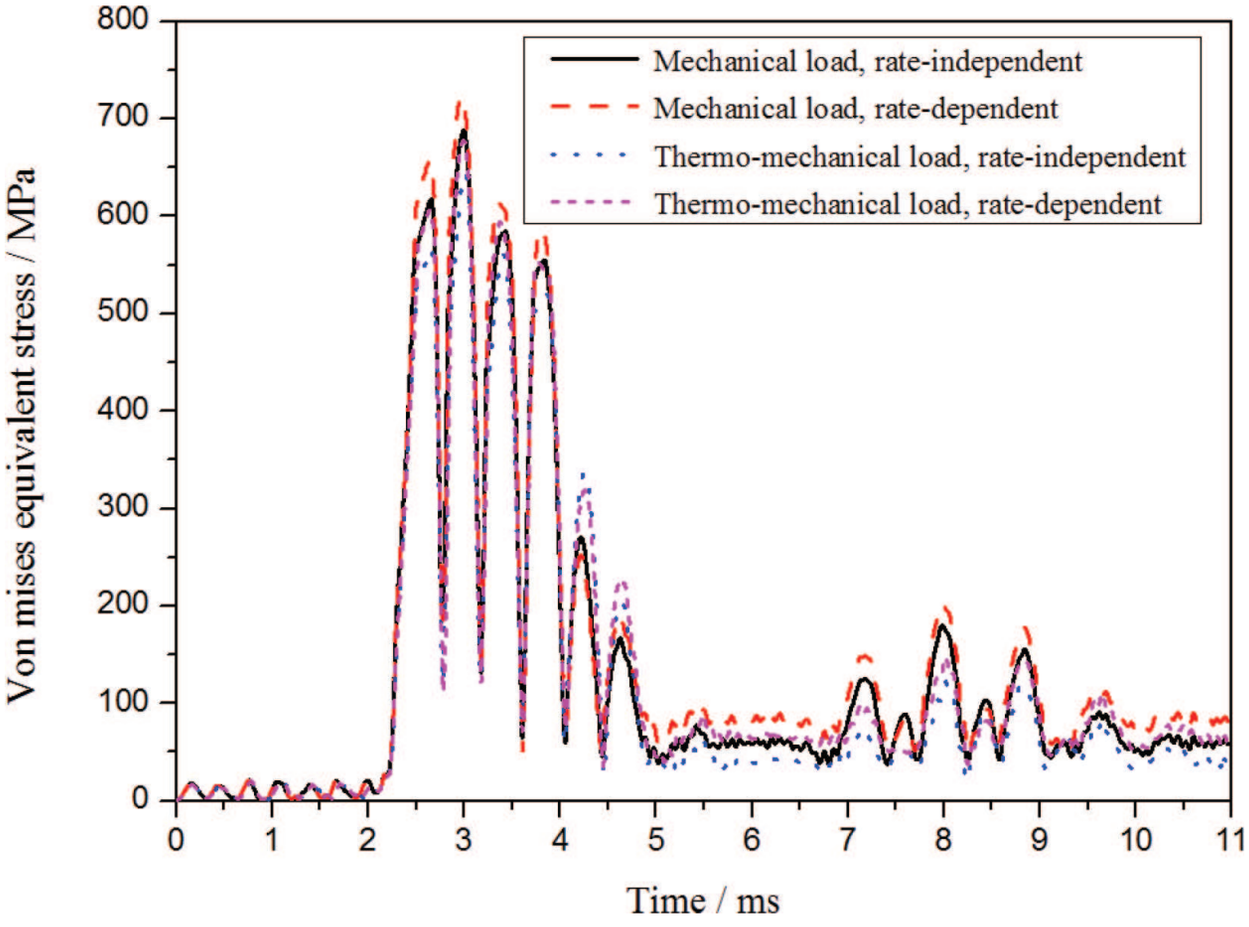

Figure 10. Von Mises equivalent stress history curves under mechanical and thermo-mechanical loads.

weaken the load-carrying capability of wheel/rail materials under thermo-mechanical load, resulting in a lower von Mises equivalent stress value than that under pure mechanical load.

The accumulated equivalent plastic strains for four various studied conditions are plotted as the curves in **Figure 11**. The maximum equivalent plastic strains are occurred at the wheel tread for all conditions, and with the largest value of 2.02%. The initial thermal stress contributes to exacerbate the plastic deformation of the wheel tread, while the strain rate hardening effect of wheel/rail materials will restrain the plastic deformation.

6.2. Influence of train speed on wheel-rail impact responses

The maximum wheel-rail impact forces induced by two lengths of flat (i.e., 40 mm and 60 mm) under mechanical and thermo-mechanical loads are plotted in **Figure 12** as a function of train speed. The maximum wheel-rail impact forces are shown to be insensitive to the strain rate of wheel/rail materials under the same loading condition for each train speed. However, the maximum wheel-rail impact forces under thermo-mechanical load are less than those values under pure mechanical load, regardless of the strain rate; this is attributed to the initial thermal stress, as stated earlier. Besides, the maximum wheel-rail impact forces first increase with the increasing train speed until reaching the peak value at the speed of 150 km/h, and then decrease with the increasing train speed for the train speed beyond

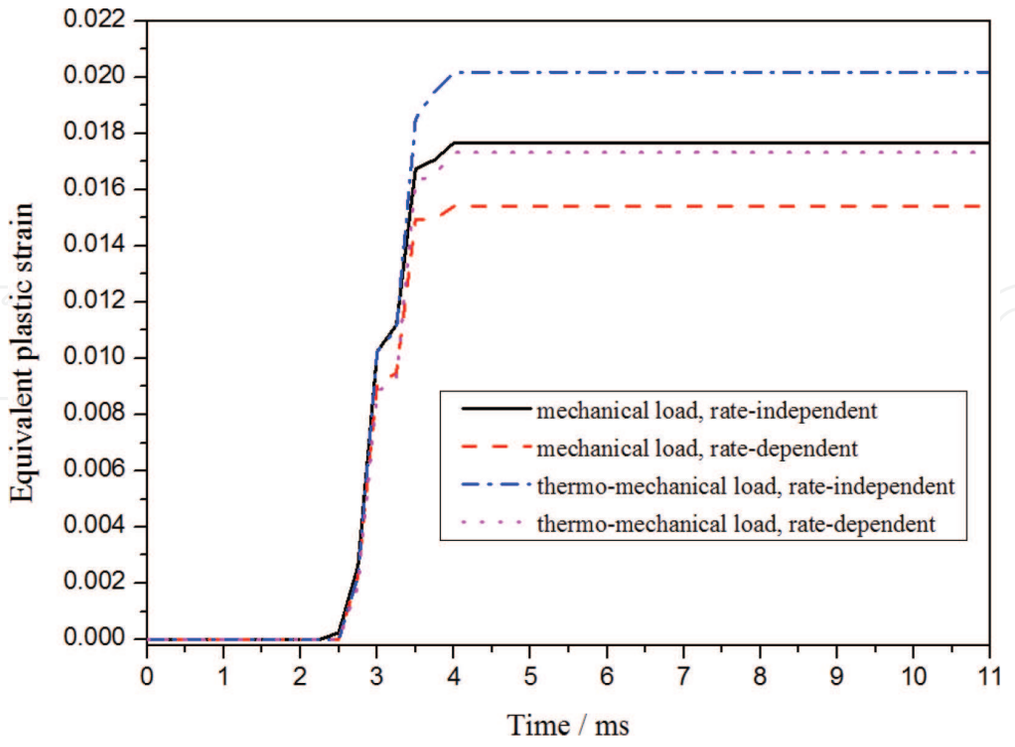

Figure 11. Equivalent plastic strain history curves under mechanical and thermo-mechanical loads.

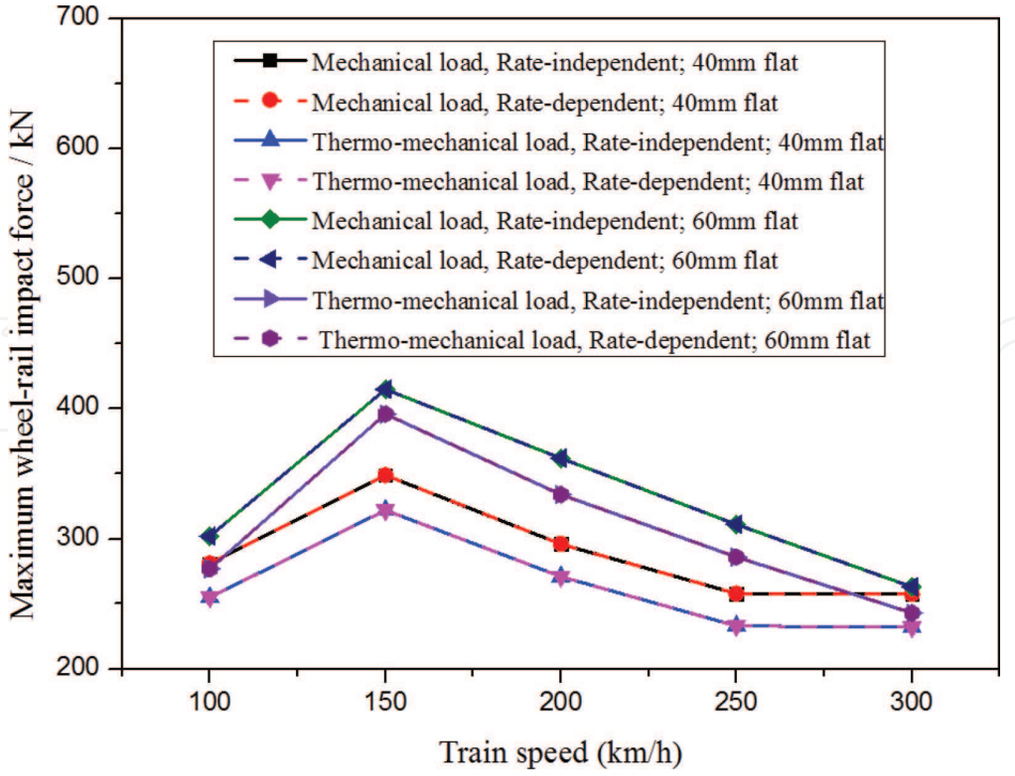

Figure 12. The maximum wheel-rail impact forces as a function of train speed.

150 km/h. This phenomenon may be explained reasonably with the dynamic contact loss opinion [2, 8]: when the wheel flat impacted against the rail, the impulse of the wheel rapidly transferred to the momentums of the wheel and rail; then the wheel tended to move upwards while the rail tended to move downwards, resulting in the loss of dynamic contact. For the lower train speed, the initial impulse of the wheel is low, and the momentums of the wheel and rail are also low; the quasi-static wheel load can maintain the wheel-rail contact, so the wheel-rail impact force increases with the train speed. However, for the higher speed case, the large impulse induces the large momentums of the wheel and rail; during the downward movement of the rail, the wheel still keeps falling for a while because of its large inertia, so the maximum impact force is attenuated, as a result of the reduction of the dynamic contact.

Figures 13–15 show the relationships of maximum von Mises equivalent stress, maximum equivalent plastic strain and maximum XY shear stress of the wheel with train speed, respectively. As shown in **Figure 13**, the maximum von Mises equivalent stress presents a similar change tendency versus train speed with that of the wheel-rail impact force, but it presents large strain rate sensitivity (i.e., the strain rate hardening effect elevates the maximum von Mises equivalent stress values under all train speed conditions). Under thermo-mechanical load, the maximum von Mises equivalent stresses are obviously greater than those under pure mechanical load. In **Figure 14**, the maximum equivalent plastic strain first increases and then decreases with the increasing train speed, and the corresponding peak value is occurred at the train speed of 200 km/h, for each loading condition. The strain rate effect of wheel/rail materials contributes to restrain the plastic deformation, resulting in a lower equivalent plastic strain value. It is interesting that the maximum equivalent plastic strains

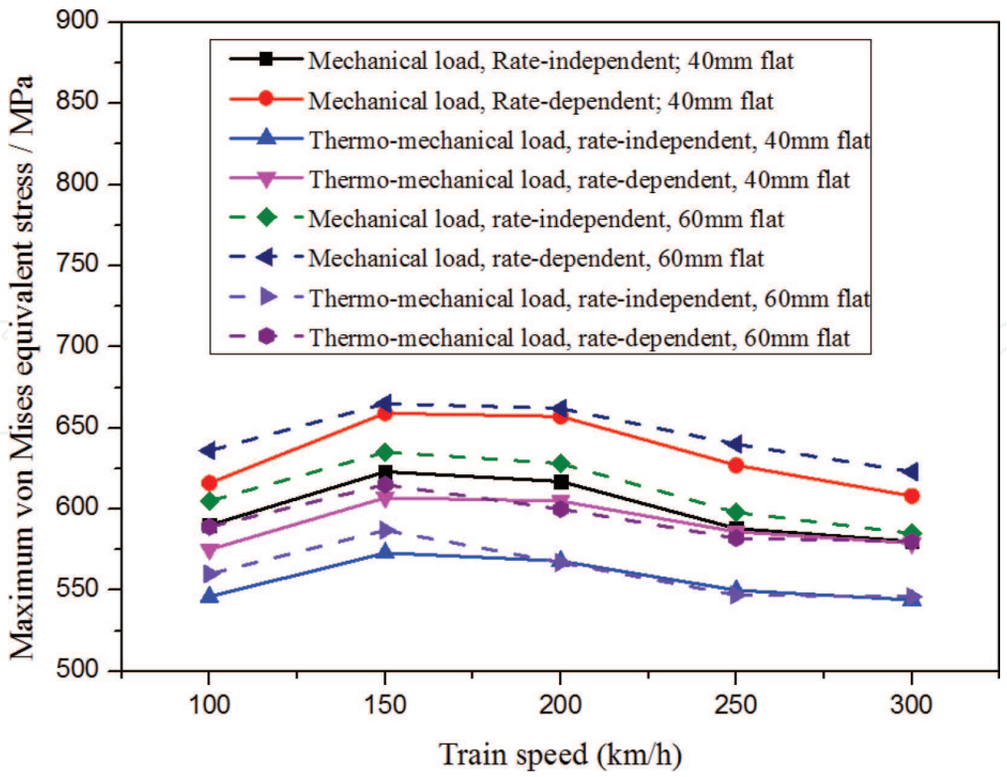

Figure 13. Maximum von Mises equivalent stresses as a function of train speed.

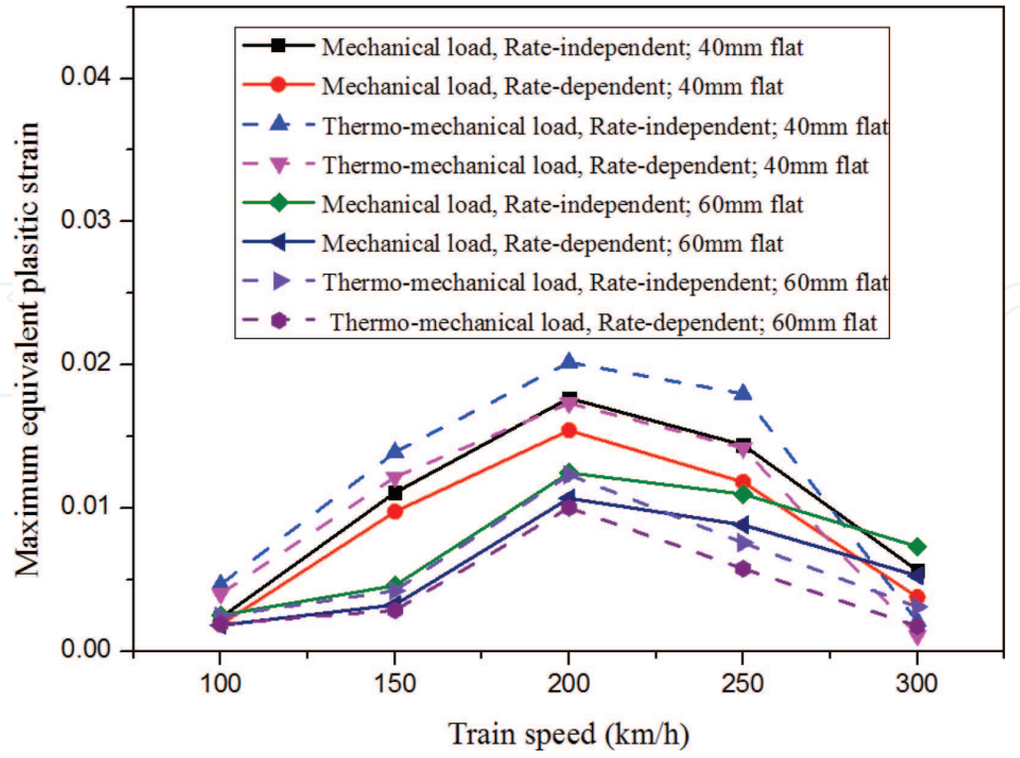

Figure 14. Maximum equivalent plastic strains as a function of train speed.

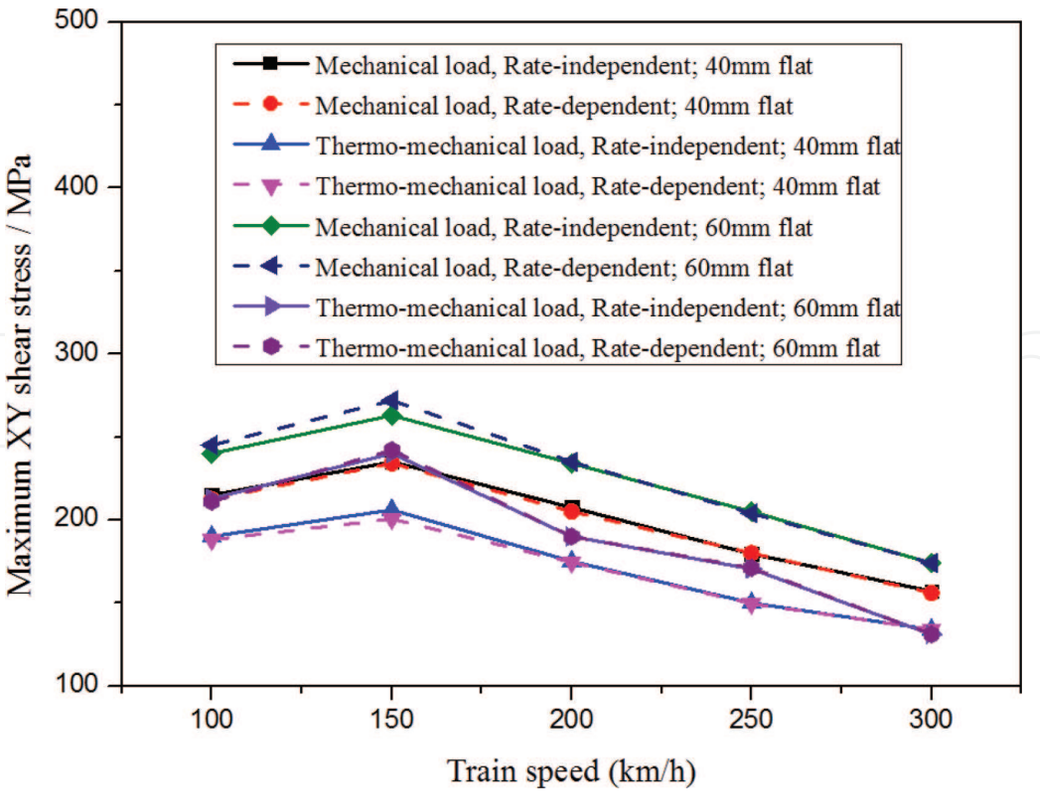

Figure 15. Maximum XY shear stresses as a function of train speed.

under thermo-mechanical load are less than those under pure mechanical load at the speed of 300 km/h. This abnormal tendency indicates that the impact position of the wheel flat has changed obviously under the speed of 300 km/h, since the equivalent plastic strain is not only related to the impact force but also the impact position. It can be found from **Figure 15** that the maximum XY shear stresses present weak strain rate sensitivity, especially with the increase of train speed; and they are lower under thermo-mechanical load than those under mechanical load for each speed condition.

6.3. Influence of flat length on wheel-rail impact responses

Based on **Figures 12–15**, the influence of flat length on the wheel-rail impact responses can be also identified. The maximum wheel-rail impact forces for each condition are revealed to be increased with the increasing the flat length. Similarly, the strain rate effect contributes to elevating the maximum von Mises equivalent stress, restraining the plastic deformation and has no effect for the XY shear stress at each condition; the initial thermal stress can decrease the maximum von Mises equivalent stresses and maximum XY shear stresses, and aggravate the plastic deformation. With the increase of flat length, the maximum von Mises equivalent stresses and the maximum XY shear stresses increase, and the maximum equivalent plastic strains decrease correspondingly.

6.4. Influence of axle load on wheel-rail impact responses

For a given train speed of 200 km/h and flat length of 60 mm, five different axle loads (i.e., 15t, 16t, 17t, 18t and 19t) are imposed to the wheel-rail contact model, to explore the influence of axle load. The maximum wheel-rail impact forces are increase approximately linearly with

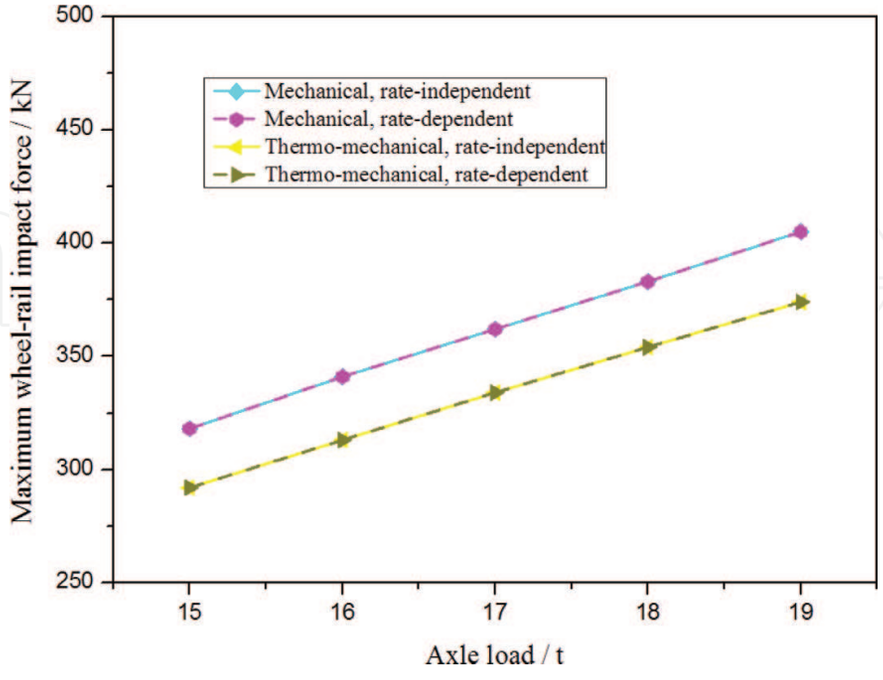

Figure 16. Maximum wheel-rail impact forces as a function of axle load.

the increasing axle load, and the values under thermo-mechanical load are lower than those under mechanical load, as shown in **Figure 16**.

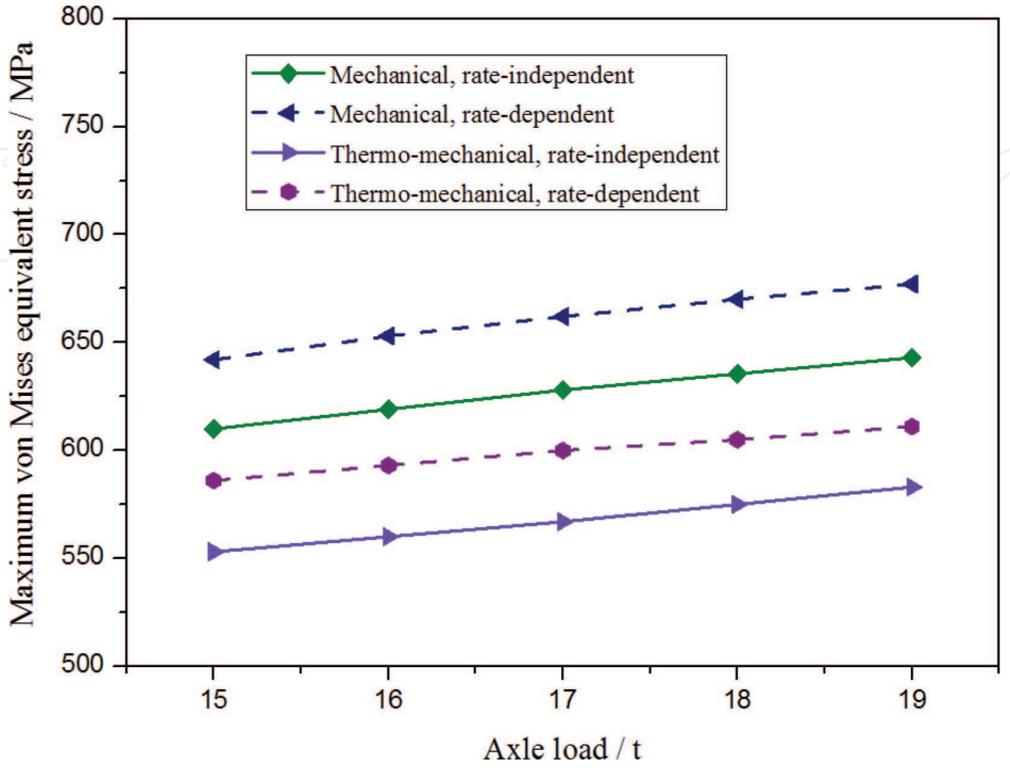

Figure 17. Maximum von Mises equivalent stresses as a function of axle load.

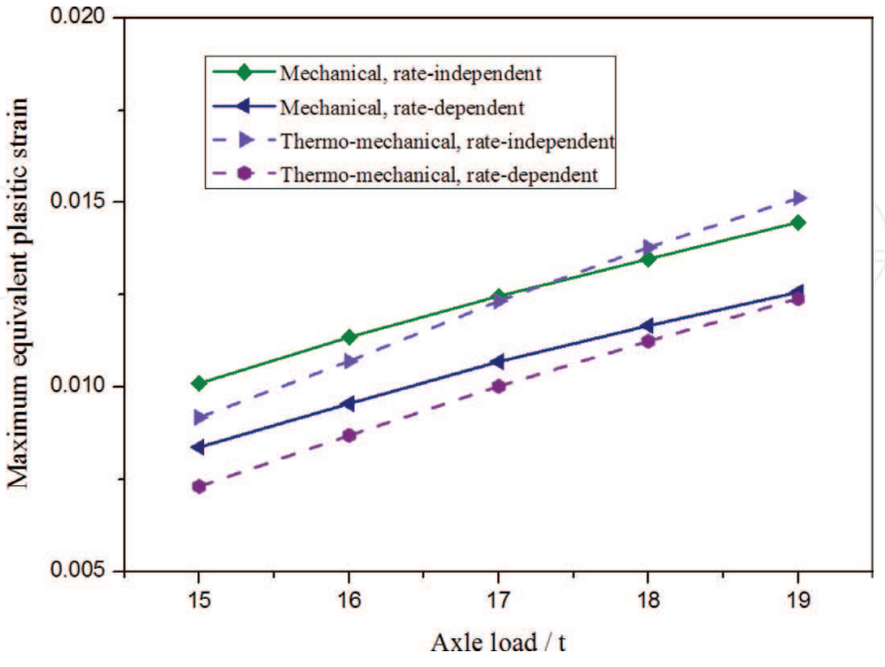

Figure 18. Maximum equivalent plastic strains as a function of axle load.

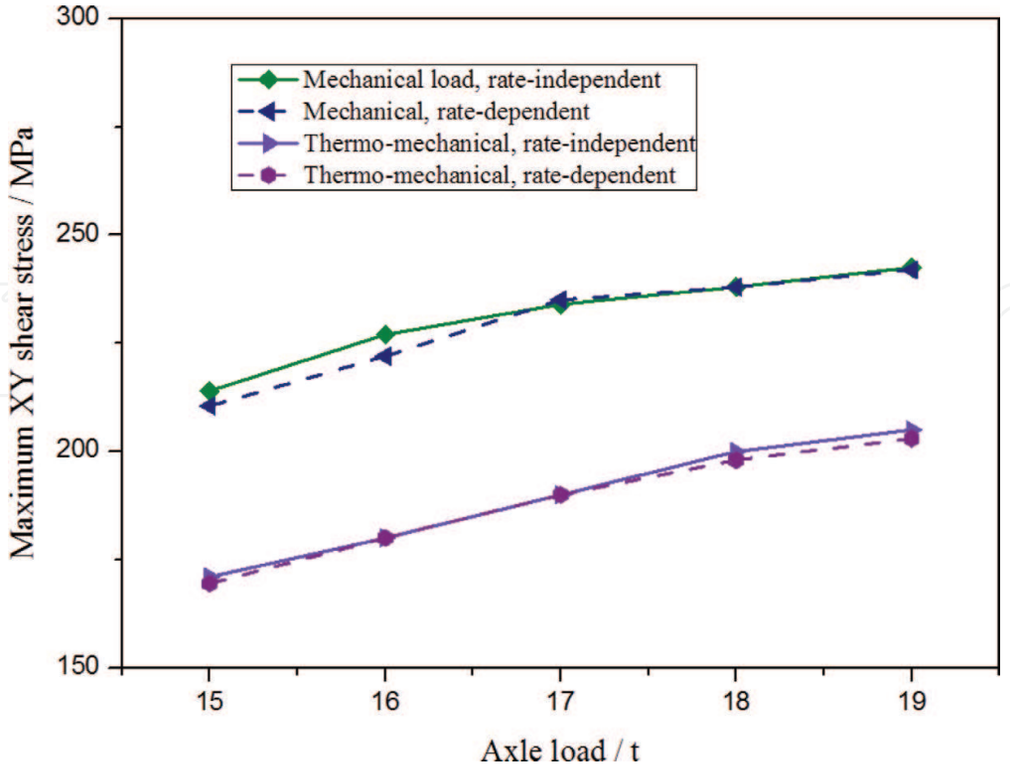

Figure 19. Maximum XY shear stresses as a function of axle load.

The maximum von Mises equivalent stress and maximum equivalent plastic strain are increased approximately linearly with the increasing axle load, while the maximum XY shear stress is increased with the axle load, as shown in **Figures 17–19**. The maximum von Mises equivalent stress increases significantly and the maximum equivalent plastic strain decreases correspondingly for each axle load case, as the strain rate effect considered. However, the strain rate has almost no influence on the maximum XY shear stress for all axle load conditions.

7. Conclusions

A 3-D wheel-rail rolling contact finite element model with a fresh wheel flat is built, and a comprehensive dynamic simulation method is used to investigate the wheel-rail impact responses. Inertia effect, strain-rate effect and temperature effect are included in the present simulation. Influences of train speed, flat length and axle load on the flat-induced wheel-rail impact responses were discussed in term of wheel-rail impact force, von Mises equivalent stress, equivalent plastic strain and XY shear stress. Some main conclusions can be drawn out:

1. The FEM-based wheel-rail rolling contact simulation can well characterise the actual geometrical and kinematic characteristics of the wheel-rail system, and well describe the strong nonlinearities in geometry, contact and material.
2. With the continuous raising of train speed, the structural inertia effect and strain rate effect of materials cannot be ignored in wheel-rail impact simulations, the thermal stress induced

by induced by the friction temperature rising during the wheel-rail sliding process also play a more important role in the wheel-rail interaction.

3. The strain rate hardening effect contributes to elevate the von Mises equivalent stress and restrain the plastic deformation; and the initial thermal stress due to the sliding friction will aggravate the plastic deformation of wheel and rail.

4. The wheel-rail impact responses first increases and then decreases with the train speed; however, they are increased with the increasing axle load. With the increase of flat length, the maximum impact force, von Mises equivalent stresses and XY shear stresses increase, and the maximum equivalent plastic strains decrease correspondingly.

Acknowledgements

The authors greatly appreciate the financial support by the National Natural Science Foundation of China (Grant no. 51475392), the Fundamental Research Funds for the Central Universities (Grant no. 2682015RC09) and the Research Fund of State Key Laboratory of Traction Power (Grant no. 2015TPL_T02).

Author details

Lin Jing

Address all correspondence to: jinglin_426@163.com; jinglin@home.swjtu.edu.cn

State Key Laboratory of Traction Power, Southwest Jiaotong University, Chengdu, P.R. China

References

[1] Newton SG, Clark RA. An investigation into the dynamic effects on the track of the wheel flats on railway vehicles. Journal of Mechanical Engineering Science. 1979;**21**(4):287-297

[2] Pieringer A, Kropp W, Nielsen JCO. The influence of contact modelling on simulated wheel/rail interaction due to wheel flats. Wear. 2014;**314**(1):273-281

[3] Steenbergen MJMM. The role of the contact geometry in wheel–rail impact due to wheel flats. Vehicle System Dynamics. 2007;**12**(45):1097-1116

[4] Johansson A, Nielsen JCO. Out-of-round railway wheels-wheel rail contact forces and track response derived from field tests and numerical simulations. Proceedings of the Institution of Mechanical Engineers Part F: Journal of Rail & Rapid Transit. 2003;**217**(2):135-146

[5] Jing L, Han LL. Further study on the wheel–rail impact response induced by a single wheel flat: The coupling effect of strain rate and thermal stress. Vehicle System Dynamics. 2017. DOI: 10.1080/00423114.2017.1340651

[6] Steenbergen MJMM. Wheel-rail interaction at short-wave irregularities [Doctoral thesis]. Delft: Netherlands, Delft University of Technology; 2008

[7] Han LL, Jing L, Zhao LM. Finite element analysis of the wheel–rail impact behavior induced by a wheel flat for high-speed trains: The influence of strain rate. Proceedings of the Institution of Mechanical Engineers Part F: Journal of Rail & Rapid Transit. 2017. DOI: 10.1177/0954409717704790

[8] Wu TX, Thompson DJ. A hybrid model for the noise generation due to railway wheel flats. Journal of Sound & Vibration. 2002;**251**(1):115-139

[9] Uzzal RUA, Ahmed AKW, Bhat RB. Modelling, validation and analysis of a three-dimensional railway vehicle-track system model with linear and nonlinear track properties in the presence of wheel flats. Vehicle System Dynamics. 2013;**51**(11):1695-1721

[10] Pletz M, Daves W, Ossberger H. A wheel set/crossing model regarding impact, sliding and deformation—Explicit finite element approach. Wear. 2012;**294-295**:446-456

[11] Zhao X, Wen ZF, Zhu MH. A study on high-speed rolling contact between a wheel and a contaminated rail. Vehicle System Dynamics. 2014;**10**(52):1270-1287

[12] Polach O. Creep forces in simulations of traction vehicles running on adhesion limit. Wear. 2005;**258**:992-1000

[13] Torstensson PT, Nielsen JCO. Simulation of dynamic vehicle–track interaction on small radius curves. Vehicle System Dynamics. 2011;**49**:1711-1732

[14] BS-EN-13104 Standard. Railway applications-Wheelsets and bogies-Powered axles-Design method; 2009

[15] LS-DYNA Theory Manual. Livermore Software Technology Corporation; California, 2006

[16] Jing L, Su XY, Zhao LM. The dynamic compressive behaviour and constitutive modelling of D1 railway wheel steel over a wide range of strain rates and temperatures. Results in Physics. 2017;**7**:1452-1461

[17] Tian Y, Cheng YR, Liu XW. Studies on the dynamic behaviour of U71Mn rail steel under high strain rates. China Railway Science. 1992;**13**:34-42

IntechOpen